

Model analysis of urbanization impacts on boundary layer meteorology under hot weather conditions: a case study of Nanjing, China

Lei Chen^{1,3} · Meigen Zhang¹ · Yongwei Wang²

Received: 29 June 2014 / Accepted: 8 June 2015 / Published online: 2 July 2015
© Springer-Verlag Wien 2015

Abstract The Weather Research and Forecasting (WRF) model, configured with a single-layer urban canopy model, was employed to investigate the influence of urbanization on boundary layer meteorological parameters during a long-lasting heat wave. This study was conducted over Nanjing city, East China, from 26 July to 4 August 2010. The impacts of urban expansion and anthropogenic heat (AH) release were simulated to quantify their effects on 2-m temperature, 2-m water vapor mixing ratio, and 10-m wind speed and heat stress index. Urban sprawl increased the daily 2-m temperature in urbanized areas by around 1.6 °C and decreased the urban diurnal temperature range (DTR) by 1.24 °C. The contribution of AH release to the atmospheric warming was nearly 22 %, but AH had little influence on the DTR. The urban regional mean surface wind speed decreased by about 0.4 m s⁻¹, and this decrease was successfully simulated from the surface to 300 m. The influence of urbanization on 2-m water vapor mixing ratio was significant over highly urbanized areas with a decrease of 1.1–1.8 g kg⁻¹. With increased urbanization ratio, the duration of the inversion layer was about 4 h shorter,

and the lower atmospheric layer was less stable. Urban heat island (UHI) intensity was significantly enhanced when synthesizing both urban sprawl and AH release and the daily mean UHI intensity increased by 0.74 °C. Urbanization increased the time under extreme heat stress (about 40 %) and worsened the living environment in urban areas.

1 Introduction

A rapid increase of the global mean air temperature has been observed since the 1970s, the majority of which can be attributed to changes in anthropogenic greenhouse gases (GHGs), aerosol loading, and land use land cover (LULC) (IPCC 2007). Future climate predictions indicate an increase in the frequency and intensity of extreme weather events, such as heat waves, with global warming (Meehl and Tebaldi 2004; Della-Marta et al. 2007). The impact on human comfort and health should not be neglected when considering severe anomalous weather scenarios (McMichael et al. 2006), especially when urban areas are continuously growing through the process of urbanization.

Urbanization, an extreme example of LULC change caused by human activities, is rapidly increasing globally. It increases surface roughness by forming urban canopy layers, decreases evapotranspiration by changing land cover from vegetated or natural surfaces to impervious surfaces, influences the surface energy balance by absorbing and reflecting solar radiation, and modifies thermal and dynamic characteristics by discharging additional anthropogenic heat (AH). These changes will certainly lead to modifications of the planetary boundary layer (PBL) structure in and around urban areas by perturbing the wind, temperature, moisture, and turbulence (Miao et al. 2009). This would then change local and regional weather and climate and impact the transport and distribution

✉ Meigen Zhang
mgzhang@mail.iap.ac.cn

Lei Chen
chenlei@mail.iap.ac.cn

Yongwei Wang
wyw@nuist.edu.cn

¹ State Key Laboratory of Atmospheric Boundary Layer Physics and Atmospheric Chemistry (LAPC), Institute of Atmospheric Physics, Chinese Academy of Sciences, Beijing 100029, China

² Atmospheric Environment Center, Nanjing University of Information Science and Technology, Nanjing 210044, Jiangsu, China

³ University of Chinese Academy of Sciences, Beijing 100049, China

of air pollutants (Arnfield 2003; Parker 2006; Miao et al. 2011; Wang et al. 2014).

The percentage of the total human population that lives in cities continues to grow. The World Health Organization reported that the urban population in 2014 accounted for 54 % of the total global population, up from 34 % in 1960. This percentage is expected to increase continuously and rapidly in the coming decades (Martine and Marshall 2007). Therefore, estimation of the impacts of urbanization on the local and regional boundary layer and human comfort and health, especially in extreme weather conditions (such as heat wave events), is an important research topic.

A variety of studies have been carried out to research the effects of urbanization on urban climate and the meteorological background (Jones et al. 1990; Tran et al. 2006; Miao et al. 2011; Zhang et al. 2011; Wang et al. 2012; Yang et al. 2014). Based on a reanalysis of global weather data over the past 50 years, Kalnay and Cai (2003) showed that half of the observed decrease in diurnal temperature range (DTR) was due to urbanization in the continental USA. Jones et al. (2008) used sea surface temperature data in place of a rural network because there were few truly rural sites to assess urban-related warming over China. Their results showed a warming trend of about 0.1 °C per decade caused by urbanization over the period 1951–2004. Xu et al. (2009) and Yu et al. (2013) analyzed observational data from the Beijing meteorological tower and found a significant increase in air temperature related to urbanization over the last few decades. Azorin-Molina et al. (2014) showed that urbanization strengthened the observed atmospheric wind speed decline in three major Spanish cities, using near-surface wind speed trends recorded at 67 land-based stations. The dramatic development of computational capacity has enabled modeling research that can provide quantitative conclusions from a new perspective. Feng et al. (2012) assessed the impact of urbanization with the Weather Research and Forecasting (WRF) model, and found an increase of more than 1.44 °C in the regional average summer temperature in the Yangtze River Delta region. With and without AH emissions, Bohnenstengel et al. (2014) found that the AH flux was an important factor in the London urban heat island, using the UK Met Office Unified Model. Yang et al. (2014) suggested that urbanization played an important role in the precipitation distribution and rainfall pattern over the Milwaukee–Lake Michigan region, based on WRF modeling analyses. Chen et al. (2014) simulated a typical July heat wave in the Hangzhou province in China, and their results showed that AH release contributed about 30 % (0.22 °C) to the urban heat island effects.

Aside from changing the regional meteorology, urbanization also affects human health. Wang et al. (2012) and Fischer et al. (2012) calculated the Simplified Wet-Bulb Globe Temperature (SWBGT), a common heat stress index, to analyze the influence of urbanization on human health during heat

waves. Sherwood and Huber (2010) showed that climate warming could reduce the human body's ability to dissipate metabolic heat through the perspiration mechanism. This has a considerable knock-on effect on human thermal comfort, labor productivity, and heat-related mortality and morbidity (Kjellstrom et al. 2009).

Previous studies have used observational data to determine the influence of urbanization on weather and climate (Bornstein and Lin 2000; Lin et al. 2011). This method is limited by the number and location of meteorological stations, and uncertainties arise due to systematic errors and unique surrounding environments, such as different altitude and topography. In addition, it is difficult to designate sites as truly rural stations because of the effect of urban sprawl (Ren et al. 2007; Jones et al. 2008). Some studies considered urbanization using global climate models (GCMs) (Jin and Shepherd 2005; Oleson et al. 2010) but the resolution with a GCM is possibly too coarse to accurately describe the underlying surface characteristics of urban areas.

Therefore, a nested high-resolution mesoscale numerical model, WRF model, coupled with an urban canopy model (UCM), was employed in this work to discuss the influence of urbanization. Many researchers have shown that this combination is capable of capturing the impacts of urbanization on the local and regional meteorology (Miao et al. 2009; Shastri et al. 2014; Kang et al. 2014; Feng et al. 2014; Kusaka et al. 2014). In addition, a heat stress index (the SWBGT) was applied to determine the influence of thermal environment on human health.

This study was conducted to simulate a long-lasting heat-wave over Nanjing city, East China, from 26 July to 4 August 2010. The first aim of this paper is to demonstrate that the WRF/UCM model can accurately simulate basic meteorological fields (2-m temperature, 2-m water vapor mixing ratio, and 10-m wind speed) during the hot weather episode. The second aim is to investigate to what extent urban sprawl and AH release influence local and regional boundary layer meteorological variables. We then analyze the relationship between urbanization and the heat stress index. The results of this paper are intended to quantify how urbanization acts on extreme heat events. Understanding the impacts of urbanization on air temperature, humidity, wind speed, and heat stress intensity can improve high-temperature forecasts and enhance the adaptive capacity of Nanjing city, which is popularly known as one of the cities in “China’s four furnaces”.

2 Model and data

2.1 Study area

Our study focuses on Nanjing, the capital of Jiangsu Province in Eastern China and an important industrial production

center. Located on the broad flat alluvial plains of the Yangtze River Delta, on average the city stands about 10 m above sea level. It has a typical East Asian monsoon climate with an annual average temperature of 2–26 °C and a rain period from mid-June to July. Known as one of the hottest cities in China, the average air temperature can reach 35 °C and the extreme highest point can reach 40 °C during a summer period.

As a result of the economic reform in the late 1970s, Nanjing has experienced significant industrial and economic growth and consequently an expansion of its urban area. This is illustrated by the increase in the total non-agricultural population, which was less than 2 million in the 1990s but is now around 7 million. Furthermore, increases in both the population and the extent of the urban area are expected to continue in the future.

2.2 Synoptic background

During late July and early August 2010, a strong heat-wave swept across Nanjing city. The observed monthly mean maximum temperature from July to August was 32 °C. On the 3 August, the observed maximum temperature at the Nanjing station (58,238) reached 38.3 °C, which was the highest temperature observed by this station from 2005 to 2010. Figure 1 shows the synoptic pattern background at 1400 LST 3 August 2010 from the National Center for Environment Prediction (NCEP) reanalysis data at 500 hPa geo-potential height and 850 hPa wind field and temperature. The entirety of Nanjing city was under the control of the west Pacific subtropical high, which is usually identified by a 588 dgpm contour line at 500 hPa (Wang et al. 2002), and the subtropical high system

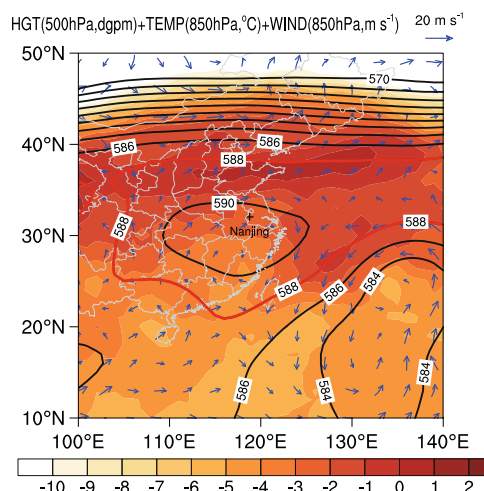


Fig. 1 The synoptic weather pattern at 1400 LST on August 3 2010 from the NCEP reanalysis data, showing geo-potential height at 500 hPa (solid lines), wind speed (arrow), and temperature (shaded) at 850 hPa. The red contour of 588 dgpm indicates the border of the western Pacific subtropical high. The black cross indicates the location of Nanjing. Units: dgpm for geo-potential height, $m s^{-1}$ for wind speed, and °C for temperature

strengthened over the next few days. This warm high pressure system produces continuous calm, cloudless, and hot weather in Nanjing.

2.3 Model configuration

In this study, we used the WRF version 3.5.1 model developed by the National Center for Atmospheric Research (Skamarock et al. 2008). The model domain was centered at (32.06° N, 118.8° E) and the horizontal grid spacings (grid numbers) of the three nested domains were 9 km (100 × 100), 3 km (85 × 85), and 1 km (97 × 97), respectively. The location of the nested domains is shown in Fig. 2a. The vertical grid contained 53 full sigma levels from the surface to 50 hPa, of which the lowest 16 levels were below 1 km for finer resolution in the planetary boundary layer. Both the initial and boundary conditions were from the NCEP operational Global Final Analyses, which had 6 h interval on a $1.0^\circ \times 1.0^\circ$ grid. The following physical parameterization schemes were employed to account for different physical processes. The Noah land-surface model, developed by Chen et al. (1996, 1997), was used to provide surface sensible and latent heat fluxes and the surface skin temperature as lower boundary conditions for WRF. The single-layer urban canopy model (SLUCM), developed by Kusaka et al. (2001) and Kusaka and Kimura (2004), was used to represent the thermal and dynamic effects of urban areas. This SLUCM takes urban geometry and AH into account in its surface energy budgets and wind shear calculation. Moreover, it has three urban categories as follows: low intensity residential, high intensity residential, and commercial. Each category has different construction materials coverage, populations, and AH values. In this paper, we only considered the default urban category (high intensity residential) for all urban areas. Other parameterizations were as follows: the Yonsei University PBL scheme (Hong et al. 2006a), the single-moment six-class graupel scheme microphysical parameterization (Hong and Lim 2006b), the Dudhia shortwave radiation scheme (Dudhia 1989), the Rapid Radiative Transfer Model long-wave radiation scheme (Mlawer et al. 1997), and the Monin–Obukhov (Janjic) surface layer scheme. The Grell 3D ensemble cumulus scheme (Grell and Devenyi 2002) was only used for the outermost domain.

Several parameters, such as the building height, the road width, and the fraction of urban landscape, were used in the SLUCM to describe the geometry shape of buildings and the structure of urban areas. Previous research has taken the default values listed in the WRF (Li et al. 2013; Wang et al. 2013b). In this study, we set these parameters following Zhang et al. (2010a, b), who generated the values from the building information database of three secondary cities: Nanjing, Suzhou, and Hangzhou. The parameters can therefore be expected to represent the typical urban morphology of

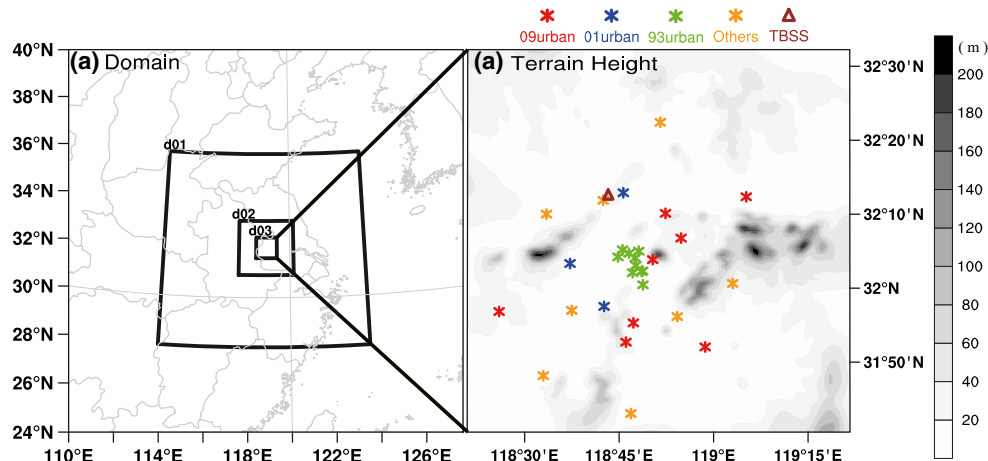


Fig. 2 Simulation domain and terrain height. **a** The configuration of the three two-way nested domains for the WRF simulation and **b** the distribution of terrain height over domain 3. The locations of the 30 AMSs (marked with asterisks) and the XLS-II TBSS (marked with triangle) are also shown. Red asterisks denote AMSs classified as urban sites in 2009 comparing the urban areas of URB09 and URB01 (the urban

areas are red grids in Fig. 4). Blue asterisks denote AMSs classified as urban sites in 2001 comparing the urban areas of URB01 and URB93. Green asterisks denote AMSs classified as urban sites in 1993 comparing the urban areas of URB93 and NOURB. Yellow asterisks denote rural sites. The brown triangle denotes the location of the TBSS. The filled areas indicate the mean terrain clearance (Unit: m)

Nanjing. We took the thermal parameters (such as the heat capacity, the thermal conductivity, and the albedo and the heat emission from the roof, wall, and ground) from Zhang et al. (2013). They optimized these values based on an off-line simulation of the surface energy balance using the WRF model. Details are listed in Table 1. The uniform morphological and thermal parameters used in our work may cause uncertainties in the simulation. Lin et al. (2008) illustrated that different values of these parameters had impacts on boundary layer development and surface air temperature. Detailed analysis and sensitivity experiments will be considered in the future research.

Another important parameter is AH, and its influence on the urban environment should not be neglected (Block et al. 2004; Narumi et al. 2009; Allen et al. 2011; Giovannini et al. 2014). Feng et al. (2012) computed the daily maximum AH release as 90, 50, and 20 W m^{-2} for three urban categories (commercial, high-intensity residential, and low-intensity residential, respectively) across Beijing-Tianjin-Hebei and the Yangtze River delta area. Chen et al. (2014) set the same values as Feng et al. (2012) in Hangzhou city. For the Beijing and Tianjin area, Zhang et al. (2013) increased the values to 110, 90, and 50 W m^{-2} for each of the urban categories, respectively. In this study, we set the daily maximum AH value as 90 W m^{-2} for the high-intensity residential category in Nanjing. This energy was treated as one part of the sensible heat flux in SLUCM (Chen et al. 2011). The diurnal AH profile is shown in Fig. 3. In section 3.2, we conducted sensitivity experiments of AH to quantify its impact on meteorological variables.

As Miao et al. (2009) and Dai et al. (2011) have shown, the influence of urbanization on air temperature reaches its maximum on calm, cloudless, and clear days. A 9-day simulation

was conducted from 2000 LST 26 July 2010 to 1900 LST 4 August 2010 and divided into three blocks. Both the first and second blocks were integrated for 85 h, while the third block was integrated for the remaining 97 h. The initial 12-h period of each simulation block was considered as a meteorological spin up to minimize the effect of the initial conditions. The model output was in the form of hourly results.

2.4 Case design

The default land use and land cover data (USGS 24 category) used in the WRF/Noah/SLUCM model was based on the 1-km Advanced Very High Resolution Radiometer data from 1992 to 1993. This database does not accurately represent the current land surface condition, especially in urban areas. Therefore, based on the original USGS land use data, we updated its urban map using 1-km Moderate Resolution Imaging Spectroradiometer (MODIS) data.

The main objective of this research is to explore the effects of urbanization on the local and regional boundary layer meteorological parameters in Nanjing. Five different scenarios (NOURB, URB93, URB01, URB09, and URB09AH) were devised for numerical experiments, as defined in Table 2. In NOURB (Fig. 4a), the entire urban surface was replaced by irrigated cropland, the most common land cover type surrounding the urban area of Nanjing. The default USGS data was used in URB93 (Fig. 4b). URB01 (Fig. 4c) was the same as URB93, except that all the urban land cover fractions were updated using the 2001 MODIS data. All urban land cover fractions were updated using the 2009 MODIS data in URB09 (Fig. 4d). URB09AH was the same as URB09, except AH was also considered. Simulations of NOURB, URB93, URB01, and URB09 with different urban maps were carried

Table 1 Summary of the parameters used in the WRF/Noah/SLUCM model

Parameters	Description	Value	Units
ZR	Building height	20	m
ROAD_WIDTH	Road width	20	m
FRC_URB	Fraction of the urban landscape occupied by artificial materials	0.9	—
CAPR/CAPB/CAPG	Heat capacity of the roof/building wall/ground	1.75E + 06	Jm ⁻³ K ⁻¹
AKSR/AKS _B /AKSG	Thermal conductivity of the roof/building wall/ground	1.5	Jm ⁻¹ s ⁻¹
ALBR/ALBB/ALBG	Surface albedo of the roof/building wall/ground	0.05	—
SPSR/SPSB/SPSG	Surface emissivity of the roof/building wall/ground	0.98	—
AH	Anthropogenic heat	90	Wm ⁻²

out to investigate the effect of urban sprawl. The results of the URB09 and URB09AH simulations were analyzed to understand the potential contribution of AH to the urban environment. All of the physics schemes were the same for the five cases.

2.5 Observation data

The observation data used to evaluate the model performance in this study were obtained from 30 Automatic Meteorological Stations (AMSSs) in Nanjing. Meteorological variables such as hourly 2-m temperature, 2-m relative humidity, and 10-m wind speed were selected, and the records were evaluated under automated quality control. In addition, one XLS-II tethered balloon sounding system (TBSS) was used to examine the profile of wind speed simulated by the WRF model. A correction of the measured wind speed was followed as described by Wang et al. (2013a). More information about XLS-II TBSS can be found in Wang et al. (2004). The locations of the 30 AMSSs and the TBSS are given in Fig. 2b.

3 Results

3.1 Model evaluation

The URB09AH case has the latest land use and land cover data including AH emission and represents the closest scenario to the actual situation of Nanjing city. Therefore, in this section, the simulation results of URB09AH are used to validate the performance of the WRF model system by evaluating it against all meteorological station observations. We investigate 2-m temperature (T_2), 2-m relative humidity (RH_2), 10-m wind speed (WS_{10}), and wind speed profiles.

The time series of the observed and simulated hourly T_2 and RH_2 averaged using data from 21 urban stations and 9 rural stations are shown in Fig. 5. The differences between observed values and those simulated for urban and rural stations are also shown. The model captures well the diurnal variations of T_2 and RH_2 at both urban and rural stations. The correlation coefficients of T_2 and RH_2 at urban and rural stations are all larger than 0.92. According to the bias of T_2 (RH_2), there is a better match in urban stations than in rural stations. The mean error is -0.05 °C (0.65 %) for urban stations and -1.25 °C (6.07 %) for rural stations. The maximum deviation in urban stations is nearly 4 °C (-14.4 %) at 1700 LST 30 July 2010. This difference was caused by the occurrence of precipitation during the period from 1500 LST 30 July to 0500 LST 31 July, so the observed T_2 (RH_2) declined (increased) swiftly. However, our model was unable to simulate this weather condition well. Further research will be carried out in the future to analyze the WRF model's simulation capability for precipitation. The bias of T_2 in rural stations is consistently negative. This underestimation of the temperature during the daytime indicates that the model may underestimate the absorbed solar radiation in rural areas. The underestimation during the night indicates that the model may overestimate the outgoing long-wave radiation or underestimate the upward surface heat flux. Unfortunately, since there is no detailed energy budget data, the real cause of this underestimation cannot be determined. However, similar results have also been noted in the previous studies (Ferretti et al. 2003;

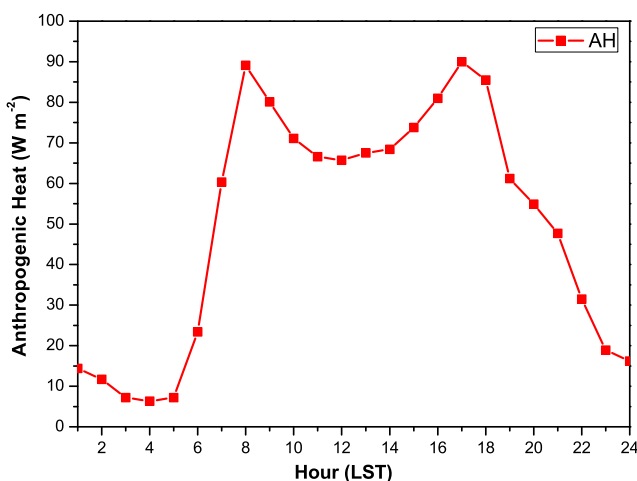
**Fig. 3** The diurnal profile of anthropogenic heat. Unit: W m⁻²

Table 2 Summary of the five cases considered

Case name	Land use and land cover map	Urbanization ratio (%)	AH option
NOURB	USGS with all urban cover replaced by irrigated cropland	0.00	OFF
URB93	USGS land use data	1.20	OFF
URB01	USGS with all urban cover updated from 2001 MODIS satellite data	6.80	OFF
URB09	USGS with all urban cover updated from 2009 MODIS satellite data	9.82	OFF
URB09AH	USGS with all urban cover updated from 2009 MODIS satellite data	9.82	ON

Miao et al. 2007). The bias of RH₂ in rural stations is positive almost consistently. This overestimation may be caused by the lower simulated T_2 , and the resultant smaller equilibrium vapor pressure of water leads to a larger relative humidity.

Figure 6 shows the time series of the observed and simulated hourly WS₁₀. The average WS₁₀ observed in urban stations is only 0.7 m s⁻¹, but the simulated result is nearly 2 m s⁻¹. The mean bias (MB) is greater than 180 %. The overestimation of WS₁₀ in urban areas occurs because of the importance of local underlying surface characteristics (Guo et al. 2011; Wang et al. 2014) and PBL schemes (Zhang and Zheng 2004; Hu et al. 2010) in WS₁₀ prediction. Additionally, calm weather conditions prevailed during the study period and this synoptic background resulted in a horizontal wind field that was weaker than observed in other time periods, especially in urban areas. As explained by Papanastasiou et al. (2010), the deviation of simulation may be large when low wind speed

is analyzed during the WRF model process. This phenomenon is very common when wind speed is analyzed in urban agglomerations under calm weather conditions. Despite this potential issue, the model can generally simulate the characteristics of the diurnal variation of WS₁₀, giving a correlation coefficient of 0.72. In rural stations, the model is more capable of reproducing the variable characteristics and magnitudes of WS₁₀; the MB is less than 0.6 m s⁻¹ and the correlation coefficient is larger than 0.88.

A further comparison between the observed and simulated wind profiles is shown in Fig. 7. The sounding data was collected by the XLS-II TBSS up to 700 m at 0200 and 1400 LST 3 August 2010. The TBSS is located at Nanjing University of Information and Science Technology (32.2° N, 118.7° E), as shown in Fig. 2b. The model can capture the vertical profile of wind speed relatively well at night, but a little deviation occurs at the height of 300–400 m in the daytime.

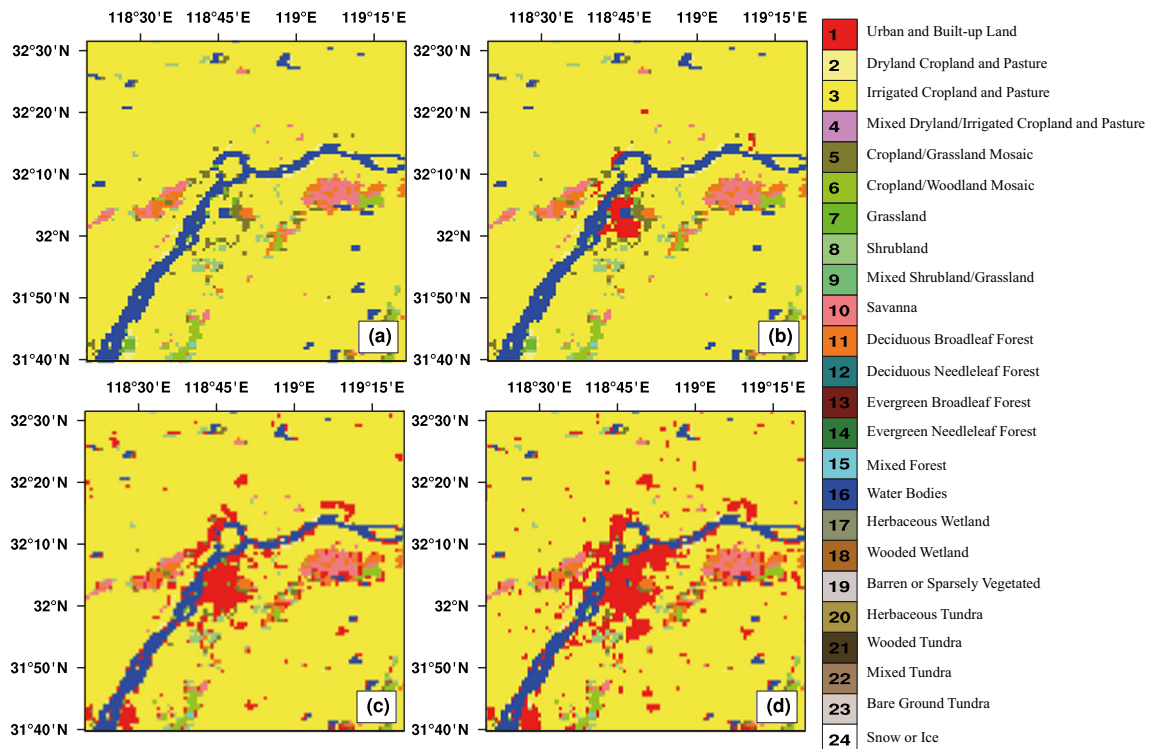
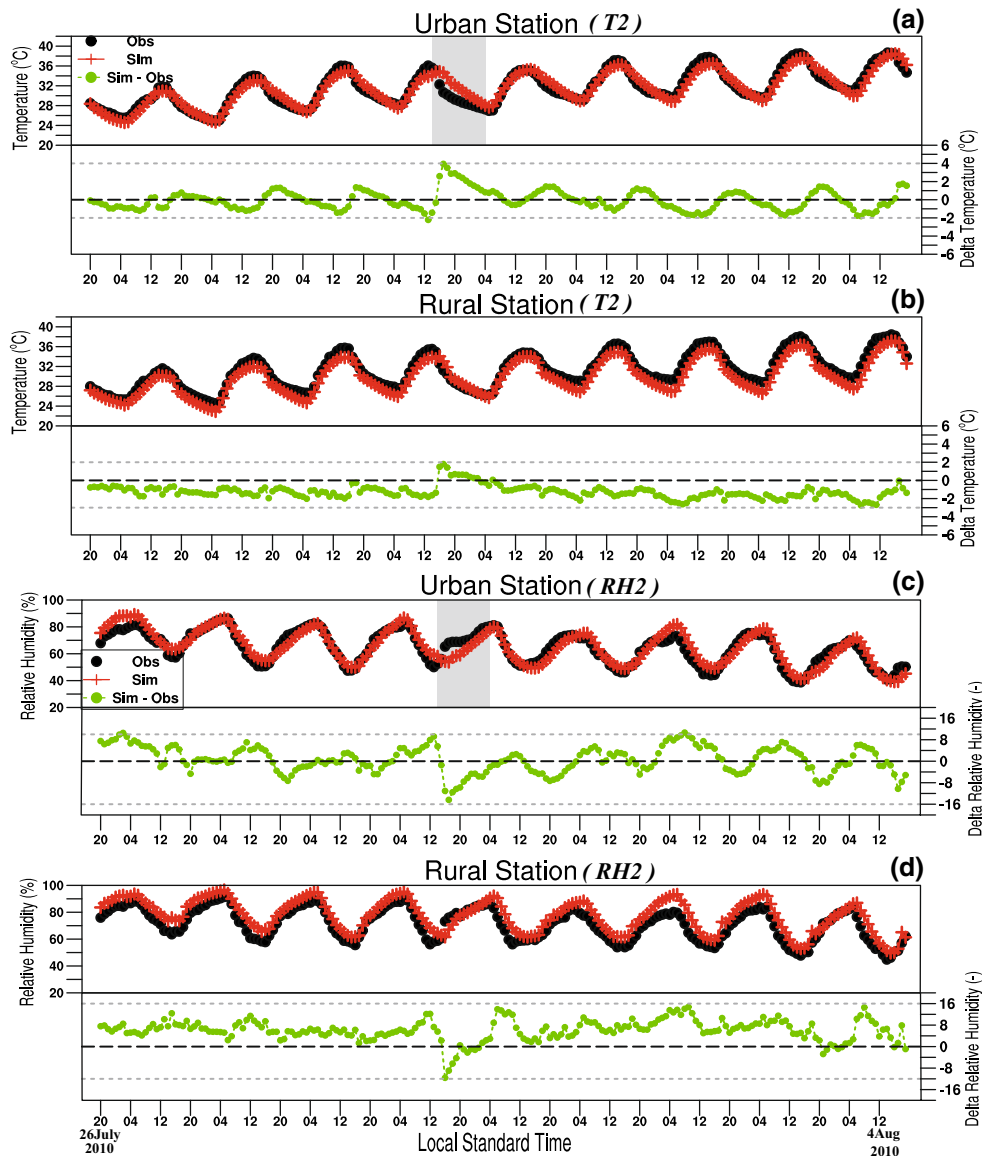


Fig. 4 Land use classification used in the WRF model for Domain 3. **a** USGS with all urban cover replaced by irrigated cropland, **b** USGS land use data, **c** USGS with all urban cover updated from 2001 MODIS satellite data, and **d** USGS with all urban cover updated from 2009 MODIS satellite data

Fig. 5 The time series of the observed (black dot) and simulated (red line and cross) 2-m temperature (T_2) and 2-m relative humidity (RH_2) averaged across 21 urban stations (**a**, **c**) and 9 rural stations (**b**, **d**) from 2000 LST July 26 2010 to 1900 LST August 4 2010. Their differences are also shown (green line and dot). The simulation results are from URB09AH and the gray shaded area from 1500 LST 30 July to 0500 LST 31 July represents the precipitation event. Units: °C for temperature and % for relative humidity



The verification statistics of T_2 , RH_2 , and WS_{10} for all five cases for the entire time period are also listed in Table 3. The average value, MB, and the root mean square error (RMSE) are calculated. Comparing with all cases, URB09AH has the lowest mean bias for T_2 (-0.36 °C) and RH_2 (1.88 %). The RMSE of RH_2 for URB09AH is also the lowest (8.60 %). The RMSE of T_2 from URB09AH is 1.79 °C, a little greater than 1.67 °C in URB01, but within the range of 0.5 °C–2.74 °C calculated by Zhang et al. (2010a, b), Zhang et al. (2011), Wang et al. (2013c), and Wang et al. (2014). This implies that the updated land surface information and consideration of AH release can improve the simulation results of T_2 and RH_2 . The mean bias of WS_{10} from URB09AH (0.97 m s $^{-1}$) is a little larger than that from URB09 (0.90 m s $^{-1}$). This is because when AH is added, more energy heats the lower atmosphere and strengthens the urban-breeze circulation.

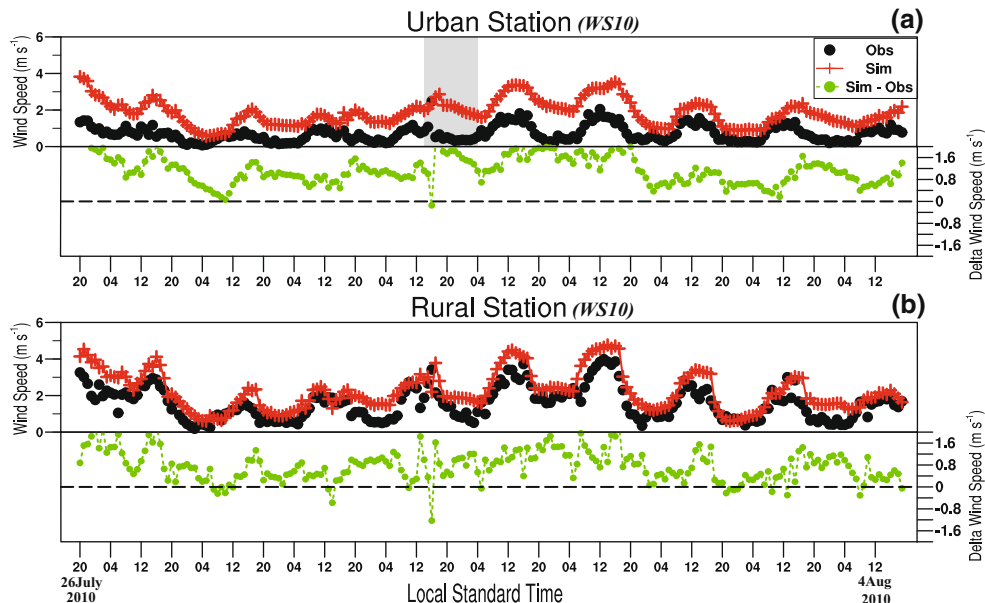
In summary, URB09AH simulated by the WRF/Noah/SLUCM model compares reasonably well with the observations. The sensitivity experiments designed in our research will next examine at the differences between each case, which can reduce the impact of systematic differences (such as different model physics schemes). We therefore believe that the WRF model is suitable and appropriate in this research.

3.2 Sensitivity experiments

3.2.1 Changes in 2-m temperature

To investigate the impact of urban expansion and AH release on T_2 , simulations from five cases are compared with each other. Figure 8a–d show the spatial differences in the 9-day average 2-m temperature. It is clear that urban expansion and

Fig. 6 The time series of the observed (black dot) and simulated (red line and cross) 10-m wind speed (WS_{10}) averaged across 21 urban stations (top) and 11 rural stations (bottom) from 2000 LST July 26 2010 to 1900 LST August 4 2010. Their differences are also shown (green line and dot). The simulation results are from URB09AH and the gray shaded area from 1500 LST 30 July to 0500 LST 31 July represents the precipitation event. Units: $m s^{-1}$



AH release have a positive effect on air temperature increase. Once the land surface type is changed from irrigated cropland to an impervious surface with a larger heat capacity and a more efficient heat transfer, there is a clear warming effect of about 1.6°C in urbanized areas on average and the maximum warming is over 2.5°C .

The simulated regional influence of urbanization can be assessed by the effect index (EI) described by Zhang et al. (2010a, b):

$$EI(x) = \frac{A_{\text{change}}(x)}{A_{\text{urban}}}, \quad (1)$$

where the variable x can be any meteorological parameter, $A_{\text{change}}(x)$ is the area in which the variable x differs between other simulations, and A_{urban} is the area in which other land use types are urbanized. Therefore, if $EI(x) < 1$, we can determine that only part of the urbanized area is affected; if $EI(x) = 1$, then the entire urbanized area is affected; if

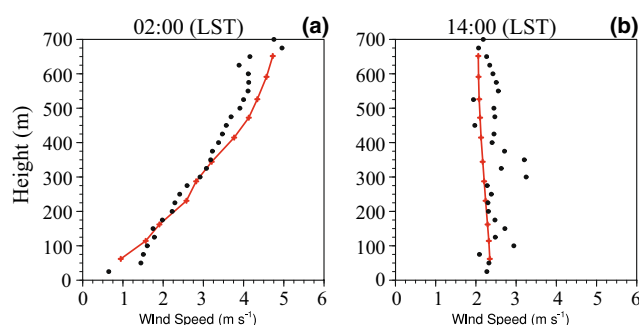


Fig. 7 Observed (black dot) and simulated (red line and dot) vertical profiles of wind speed at Nanjing University of Information and Science Technology (32.2°N , 118.7°E) at (a) 0200 and (b) 1400 LST 3 August 2010. Units: $m s^{-1}$

$EI(x) > 1$, an additional area including the newly urbanized area is affected. At the same time, we also set a threshold value to determine whether the absolute differences in the regional average value between cases are caused by the land-use change, such as 0.2°C for the air temperature. Similar handling methods were performed by Zhang et al. (2010a, b) and Wang et al. (2014). By comparing URB93 and NOURB, the warming phenomenon appears to extend outside of urban areas with an $EI = 1.8$. From cases of URB01 and NOURB, the EI is nearly 3.6, indicating a clear regional influence. For URB09 and NOURB, the EI is even larger, nearly 4.0. According to these EI values, it can be concluded that urban sprawl has a clear effect on the regional meteorological environment. In addition, the EI value increases with the growing urbanization ratio. This result represents evidence for the phenomenon of “urban shadow” caused by urbanization. Figure 8d shows the impact of AH on 2-m temperature. Because AH is only considered in urban areas in the WRF model, the mean warming in urban areas caused by AH release is about 0.34°C with an $EI = 1.1$. Generally, the average surface air temperature in the whole domain area is increased by 0.41°C due to urbanization, with a total AH contribution around 22 %.

The differences in the 9-day average 2-m maximum and minimum temperatures and diurnal temperature ranges (DTRs) are further discussed in Fig. 9. Analyzing the results from URB09 and NOURB in Fig. 9a–c, the maximum temperature at noon is increased by nearly 0.5°C in urban areas as a result of urban sprawl. The change in the minimum temperature at night is more remarkable and the highest warming in urban areas is more than 3°C . Although both the maximum and minimum temperatures are increased, the DTR is decreased by 1.24°C in urban areas on average. The decreased

Table 3 Comparison of the observed and simulated meteorological variables

Meteorological Variables	N_STD ^a	CASE	AVG ^b	MB ^c	RMSE ^d
$T_2(^{\circ}\text{C})$	30	OBS	31.39	—	—
		NOURB	29.51	-1.88	2.37
		URB93	29.91	-1.48	2.06
		URB01	30.54	-0.85	1.67
		URB09	30.77	-0.62	1.69
		URB09AH	31.03	-0.36	1.79
$RH_2(%)$	30	OBS	65.94	—	—
		NOURB	79.75	13.81	15.82
		URB92	76.15	10.21	12.75
		URB01	71.34	5.40	9.35
		URB09	69.43	3.49	8.92
		URB09AH	67.82	1.88	8.60
$WS_{10}(\text{m s}^{-1})$	30	OBS	0.98	—	—
		NOURB	2.29	1.35	1.81
		URB93	2.09	1.15	1.60
		URB01	1.90	0.97	1.43
		URB09	1.83	0.90	1.38
		URB09AH	1.95	0.97	1.44

The numbers enclosed in squares represent better results compared with other cases

SIM_i and OBS_i indicate model predictions and observations, respectively

^aN_STD is the number of stations

^bAVG indicates the mean values of observed and simulated meteorological variables

^cMB is the mean bias, $MB = \sum_{i=1}^{N_STD} (SIM_i - OBS_i) / N_STD$

^dRMSE is the root mean square error, $RMSE = \sqrt{\sum_{i=1}^{N_STD} (SIM_i - OBS_i)^2 / N_STD}$

DTR reveals that the urban thermal environment is serious not only in the daytime but also at night. Figure 9d–f reflects the contribution of AH to the 2-m maximum and minimum temperatures and DTRs. The 2-m maximum temperature increases by 0.22 °C in urban areas, and the minimum temperature increases by 0.28 °C. Although the emission of additional AH has little influence on DTR (Fig. 9f), the potential for AH to increase the near-surface air temperature should not be neglected.

3.2.2 Changes in 10-m wind speed

Urbanization increases the surface roughness because of the heterogeneous distribution of buildings and their consequent friction effect which leads to a decrease in the near-surface

wind speed. The spatial differences in the 9-day average 10-m wind speed and the change of the wind speed profiles over urban areas are shown in Fig. 10. In Fig. 10a–c, once the underlying surface type is changed, the increased surface roughness weakens WS_{10} , causing urban stilling. When comparing NOURB and the other three cases (URB93, URB01, and URB09), the decrease of 10-m wind speed in urbanized areas is similar (-0.44 m s^{-1} , -0.46 m s^{-1} , -0.47 m s^{-1} for the three comparison cases, respectively), and each scenario shows the decrease occurs on a regional scale (EI = 2.5, 3.0, 3.2 for the three comparison cases, respectively. The threshold for WS_{10} is 0.2 m s^{-1}). This reduction can also be simulated in the wind profiles up to nearly 300 m. Figure 10d shows the effect of AH release on WS_{10} . When an additional heat source is considered, the greater amount of

Fig. 8 Differences in the 9-day average 2-m temperature between **a** URB93 and NOURB, **b** URB01 and NOURB, **c** URB09 and NOURB, and **d** URB09AH and URB09. Units: °C

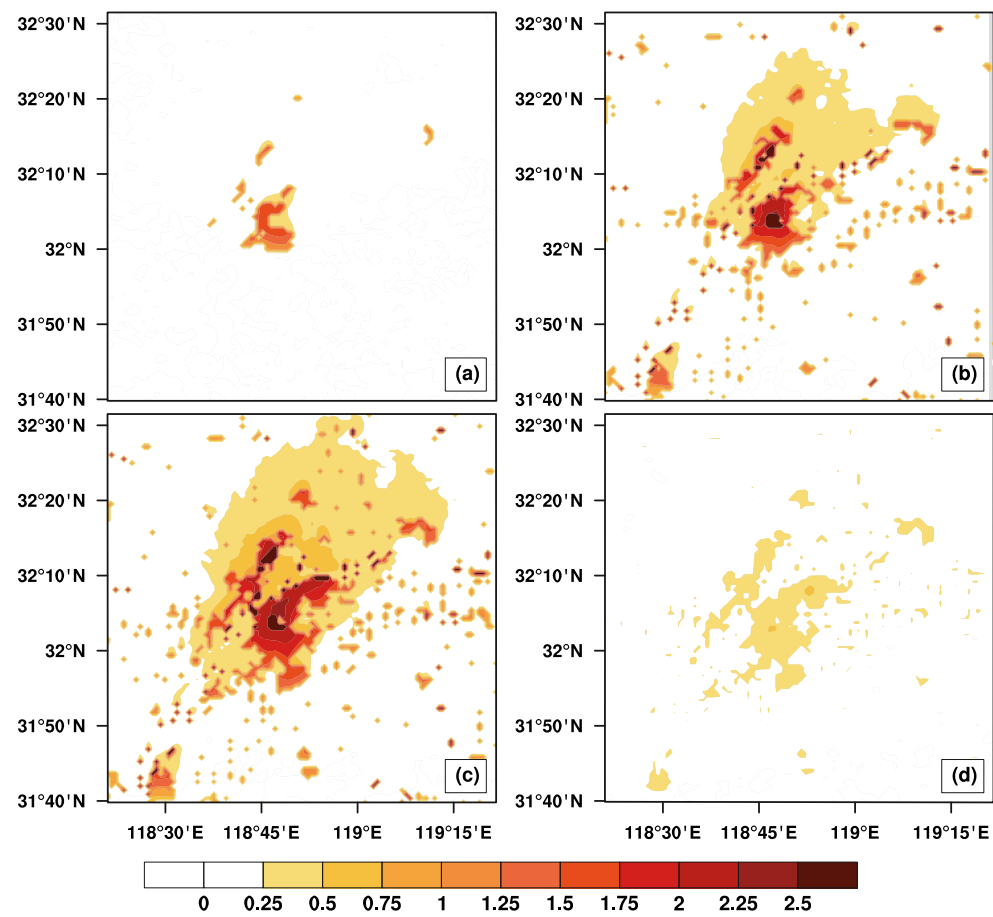


Fig. 9 Differences in the 9-day average 2-m maximum and minimum temperatures and the diurnal temperature ranges. **a, b, c** URB09 minus NOURB. **d, e, f** URB09AH minus URB09. Units: °C

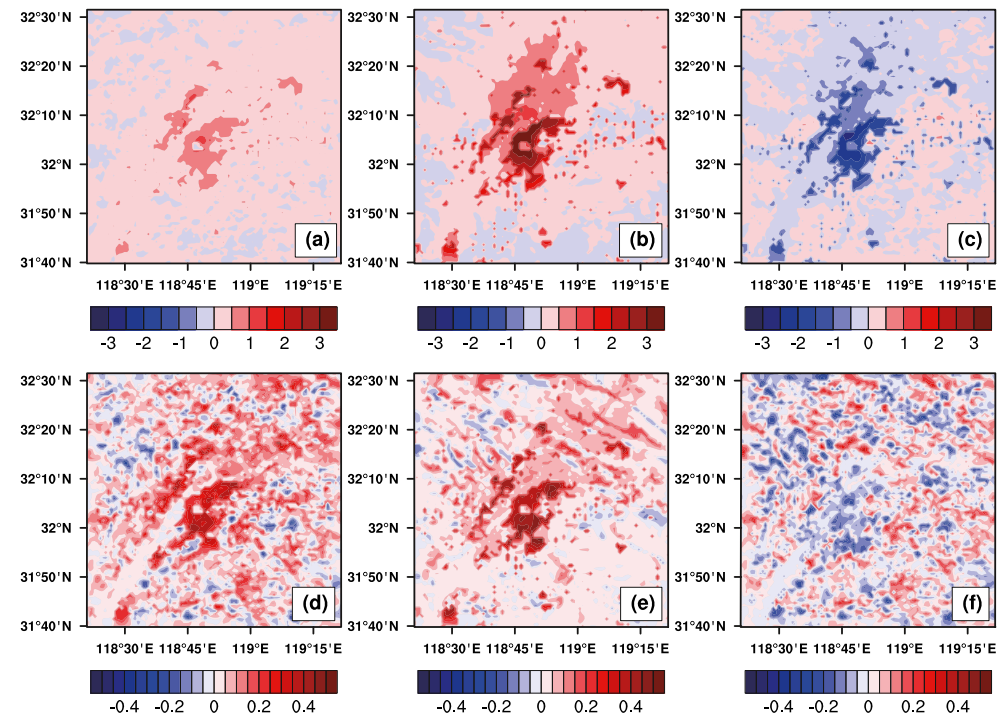
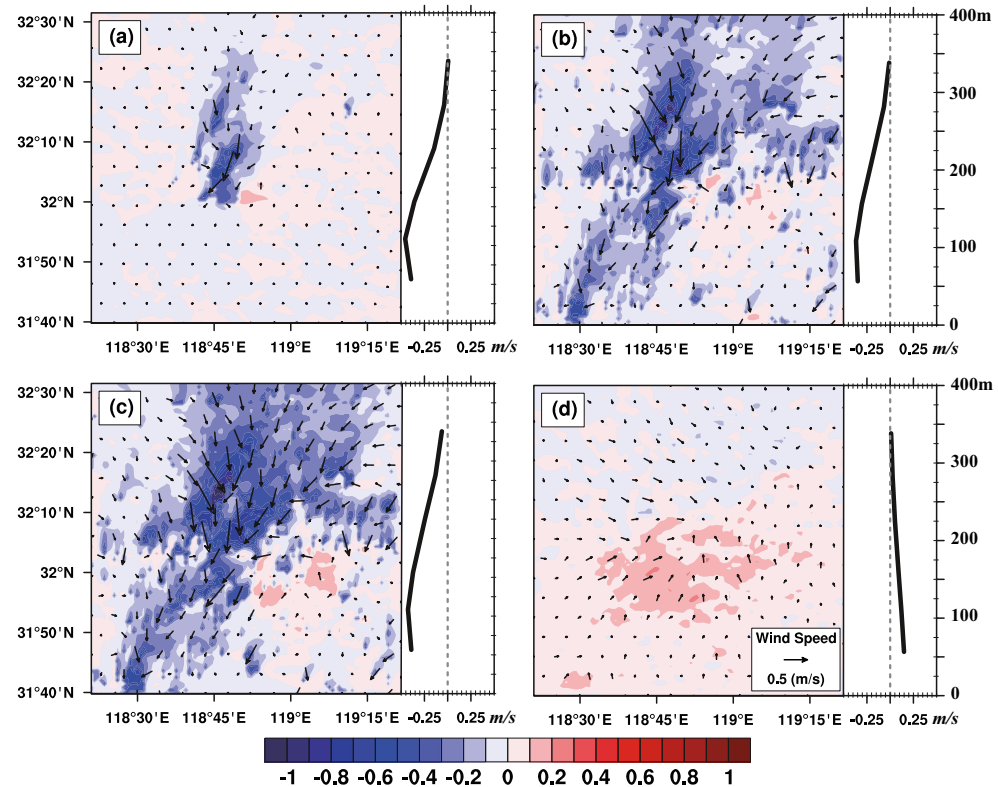


Fig. 10 Differences in the 9-day average 10-m wind speed (shaded and vectors) and the changes in wind speed profiles averaged over urban areas between **a** URB93 and NOURB, **b** URB01 and NOURB, **c** URB09 and NOURB, and **d** URB09 and URB09AH. Units: m s^{-1}



energy heats the lower atmosphere and strengthens the urban breeze circulation. In this study, the circulation increases by about 0.1 m s^{-1} in urban areas due to AH emission.

3.2.3 Impacts on surface water vapor

Urbanization changes land cover from natural land surfaces to impervious surfaces, leading to less water being available for evaporation in urbanized areas, and this may cause an “Urban Dry Island”. Figure 11 shows the impact of urbanization on the 2-m water vapor mixing ratio. The influence is significant over highly urbanized regions with a decrease of $1.1\text{--}1.8 \text{ g kg}^{-1}$ ($5.4\text{--}8.9\%$). The EI_s are 1.2 (Fig. 11a), 1.4 (Fig. 11b), and 2.0 (Fig. 11c), respectively (The threshold for RH₂ is 0.2 g kg^{-1}). However, the effect of AH on 2-m water vapor mixing ratio in urban areas is less clear (only -0.1 g kg^{-1}).

3.2.4 Changes in potential temperature

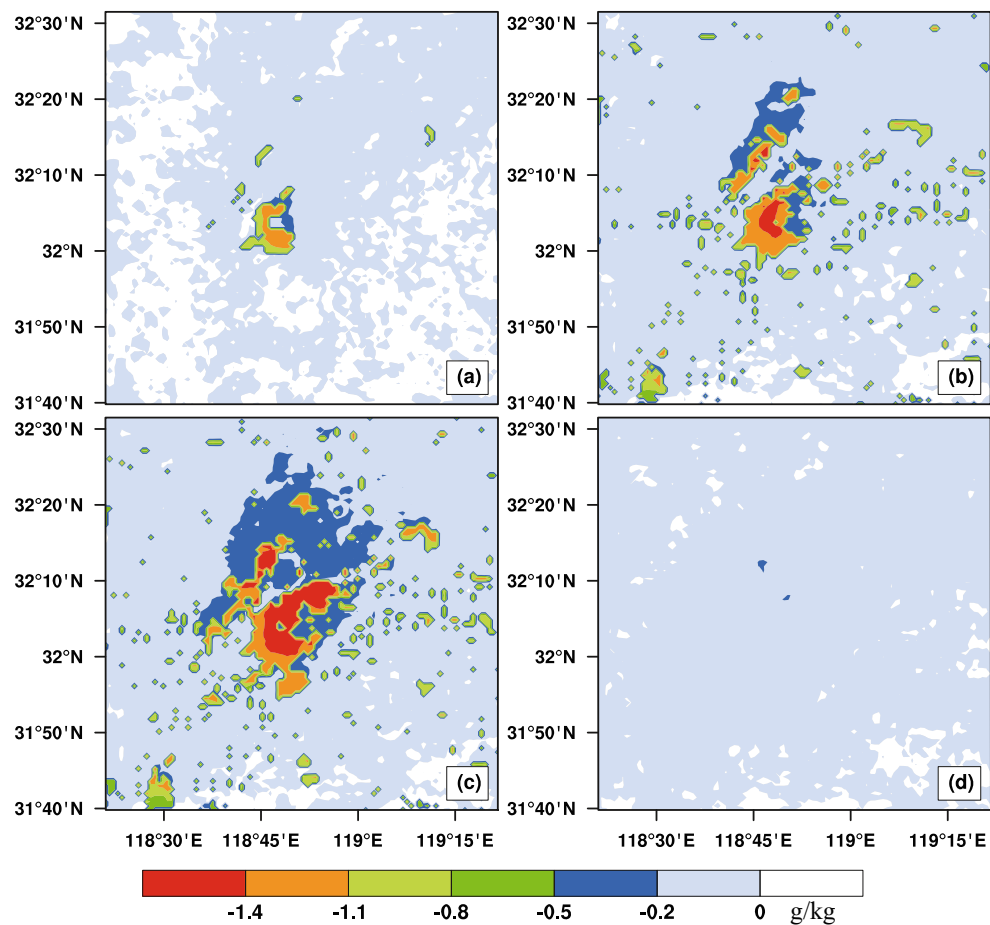
Figure 12 demonstrates the effect of urbanization on the vertical profiles of potential temperature. At night (0400 LST), thermal inversion is simulated by all cases, but the intensity decreases from NOURB (1.13°C per 100 m) to URB09AH (0.53°C per 100 m) at heights below 300 m above the urban surface (the area used to calculate the average value in NOURB is over the entire irrigated cropland), due to the increased near-surface air temperature caused by urbanization.

At 1600 (LST), more solar radiation is absorbed by the urban canopy and the lower atmosphere becomes warmer; the thermal inversion disappears and eventually forms an unstable stratification below 200 m. The intensity of the unstable layer is greater when urban sprawl and AH release are both considered (nearly -0.1°C per 100 m in URB09AH). According to the height-time section of the potential temperature averaged over urban areas (not shown), the isothermal of 35°C disappears earlier and appears later with the development of urbanization. This leads to a shorter stratification time, and the unstable stratification lasts longer. The durations of the unstable stratification are about 1 h (NOURB), 2.5 h (URB93), 3.5 h (URB01), 4 h (URB09), and 5 h (URB09AH0).

3.2.5 Changes in urban heat island intensity

Several methods exist to calculate the urban heat island (UHI) intensity. The traditional method is to calculate the difference of the near surface air temperature between the urban area and its surrounding rural areas (Miao et al. 2009; Salamanca et al. 2012; Giannaros et al. 2013). In this study, UHI intensity was calculated by subtracting the near surface air temperature in urban areas in URB93, URB01, URB09, and URB09AH (red grids in Fig. 2) from the temperature in the corresponding grids in NOURB (Wan et al. 2012; Grawe et al. 2013). The diurnal variation of the 9-day average UHI intensity is shown in Fig. 13. The simulated diurnal cycles of UHI intensity are similar or all cases. From 1700 (LST), around sunset, it grows

Fig. 11 Differences in the 9-day average 2-m water vapor mixing ratio. **a** URB93 and NOURB, **b** URB01 and NOURB, **c** URB09 and NOURB, and **d** URB09 and URB09AH. Units: g kg^{-1}



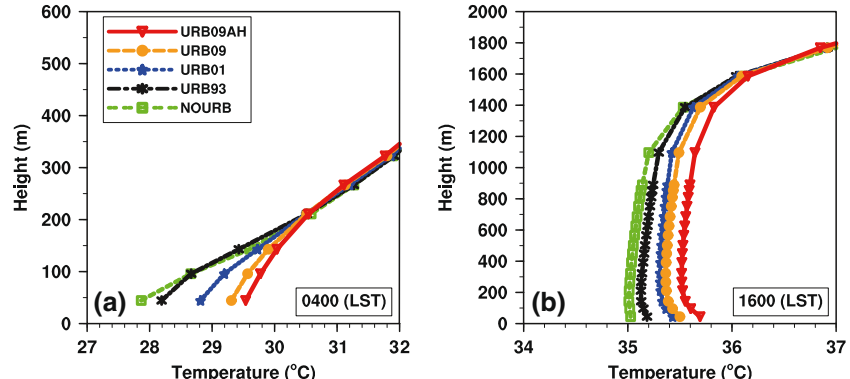
rapidly and reaches a maximum peak about $3.3\text{ }^{\circ}\text{C}$ at 1900 (LST), then UHI intensity declines slightly during the nighttime and in the early morning (at 0500 LST), it rapidly plunges. After sunrise, UHI intensity reaches the minimum about $0.26\text{ }^{\circ}\text{C}$. The daily average UHI intensities for URB93, URB01, and URB09 are 1.3 , 1.6 , and $1.7\text{ }^{\circ}\text{C}$, respectively. This shows that urban sprawl can increase the difference of air temperature between urban and rural areas. Many studies reveal that AH release has an impact on UHI intensity (Lee et al. 2009; Feng et al. 2012). In this study, when AH is considered, the daily mean UHI intensity increases by

$0.34\text{ }^{\circ}\text{C}$, and the largest increase happens at 0800 (LST) about $0.62\text{ }^{\circ}\text{C}$. This is because the emission of AH at 0800 (LST) reaches the peak value (Fig. 3).

3.2.6 Impacts of urbanization on heat stress index

As shown above, urban amplification and AH release significantly increase the air temperature in urban areas. The rising air temperature affects thermal comfort of human beings and causes heat-related health problems. Several heat stress indices (HSIs) are widely used to account for the effects of air

Fig. 12 Potential temperature profiles averaged over urban areas at **a** 0400 (LST) and **b** 1600 (LST) on 2 August 2010. The area used to calculate average values in NOURB is over the entire irrigated cropland. Units: $^{\circ}\text{C}$



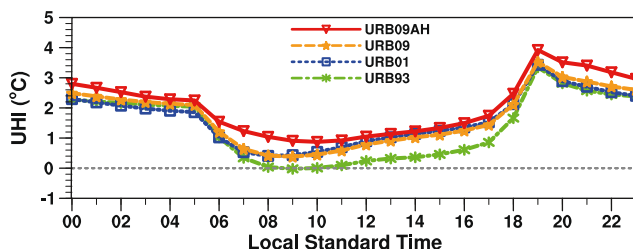


Fig. 13 Diurnal variation of the 9-day average UHI intensity. Units: °C

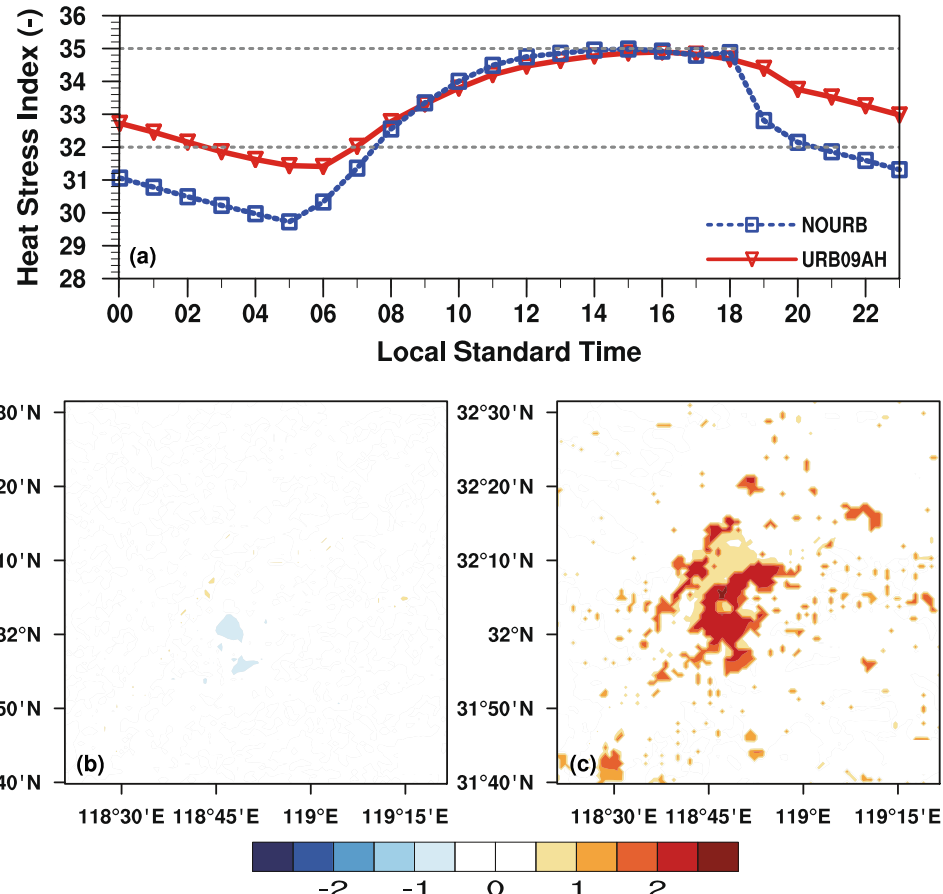
temperature in addition to further environmental factors on human health (Fischer et al. 2012). In this study, a Simplified Wet-Bulb Globe Temperature (SWBGT, hereafter denoted W) is chosen to discuss the effect of urbanization, with

$$W = 0.567 \times T + 0.393 \times e + 3.94, \quad (2)$$

where T is the air temperature in °C and e is the vapor pressure in hPa. The thresholds of W in this study are 28, 32, and 35 to represent high, very high, and extreme risk to health (Willett and Sherwood 2012), respectively. During this heat wave from 26 July to 4 August in 2010, the numbers of high, very high, and extreme heat-stress hours are 86, 88, and 42, respectively, for NOURB and 48 (decreased by 44 %), 109

(increased by 24 %), and 59 (increased by 40 %), respectively, for URB09AH. Figure 14a shows the diurnal cycles of the 9-day average heat stress index in urban areas simulated by NOURB and URB09AH (the grids used to calculate average values in NOURB are the same as in URB09AH). The maximum HSI appears in the afternoon at 1500–1600 (LST), and the minimum HSI appears in the early morning at 0500–0600 (LST). Comparing the two cases, HSIs are nearly equal in the daytime, but during the nighttime, HSI calculated by URB09AH is 1.5 unit higher than that by NOURB, in agreement with the results of Fischer et al. (2012). From 0700 to 0200 (LST) (about 83 % of the time in a day), the value of HSI is greater than 32 in the URB09AH case, compared with 54 % in NOURB case. The spatial distribution of the differences in the maximum and minimum HSI between URB09AH and NOURB in the whole domain is shown in Fig. 14b, c. The simulated urban area contrast in maximum heat stress is not apparent. This is because although urbanization increases the air temperature in urban areas, it also decreases the humidity. The warmer urban temperature and lower humidity have opposite effects on heat stress. However, the difference in the minimum HSI is clearly apparent between the two cases, especially in urban areas. The average minimum HSI in urban areas increases by about 1.6 unit. All results discussed above

Fig. 14 **a** Diurnal cycles of the 9-day average heat stress index in urban areas (The grids used to calculate average values in NOURB are the same as in URB09AH). The spatial distribution of the differences in **b** the maximum and **c** the minimum heat stress index between URB09AH and NOURB are also shown. Units: –



show that urbanization raises the risk level in urban areas and has the potential to make the living environment worse for a longer amount of time.

4 Summary and conclusions

Rapid urban expansion and increasing urban populations have caused remarkable modifications to the local underlying land use type and regional environment. The change in meteorological variables in urban areas may have serious influences on human health, especially in extreme weather events. This paper focused on the development of a next generation meso-scale model, WRF, coupled with a single urban canopy parameterization scheme. The aim was to quantify the effects of urbanization on boundary layer meteorological parameters and heat stress index over Nanjing, China, during a long lasting heat wave. Five scenarios (NOURB, URB93, URB01, URB09, and URB09AH) were integrated from 26 July to 4 August 2010. The first four cases with different urban maps were designed to compare the impacts of urban sprawl. URB09 and URB09AH were designed to analyze the contribution of AH. Model evaluation with the observed data of T_2 , RH_2 , and WS_{10} indicates that the WRF model is capable of capturing the features of urban meteorological variables over Nanjing under a hot weather episode.

The simulated results demonstrate that urban expansion has a regional influence on the 2-m temperature, and the mean increase in the urbanized areas is about 1.6 °C. The urban-average DTR decreases by -1.24 °C from NOURB to URB09, indicating a potentially dangerous urban thermal environment. The total contribution of AH release to the warming in urban areas is nearly 22 %. Urban sprawl was found to have a negative impact on 10-m wind speed, due to the increase of surface roughness in urban areas. By comparing NOURB and URB09, we showed that WS_{10} decreases by about 0.4 m s^{-1} , and this reduction can be simulated from the surface to 300 m in urban areas. However, the additional heat energy from AH release heats the atmosphere and strengthens the urban breeze circulation by about 0.1 m s^{-1} . Replacing vegetated surfaces and irrigation croplands with urban surfaces also leads to a decrease in humidity. RH_2 decreases by $1.1\text{--}1.8 \text{ g kg}^{-1}$ in highly urbanized areas but the effect of AH release on RH_2 is insignificant. Urbanization also has a large effect on potential temperature. With the urbanization of Nanjing city, the isothermal of 35 °C disappears earlier and appears later, so the duration of the inversion layer is almost 4 h shorter. Moreover, the intensity of the unstable layer increases in the late afternoon. As a result of urban expansion, UHI intensity increases from 1.3 °C (URB93), 1.6 °C (URB01) to 1.7 °C (URB09). When AH release is also considered, the UHI intensity increases by about 0.34 °C. Urbanization increases the number of extreme heat stress

hours from 42 in NOURB to 59 in URB09AH during the studied heat-wave, and the urban average minimum HSI increases by 1.6 unit, indicating a worse living environment for human beings.

In this paper, we have only considered the physical influence of urbanization (urban sprawl and AH release) on the local and regional meteorological environment, and numerous complex effects (air condition effect, drag effect) should be further considered in this process. Furthermore, different parameterization schemes or different morphological parameters of buildings used in UCM have different results. Aside from the changed meteorological variables caused by urbanization, it can also affect air quality. Therefore, further studies will be carried out to quantify the effects of parameterization schemes and morphological parameters and choose an optimal combination using up-to-date LULC data to study the influence of urbanization on air quality including the feedback effects of aerosol emission on urban meteorological environment. Furthermore, a longer simulation time should be also considered to analyze the large-scale climatic effects caused by urbanization.

Acknowledgments This work is supported by the “Strategic Priority Research Program (B)” of the Chinese Academy of Sciences (XDB05030105, XDB05030102, XDB05030103), the National Basic Research Program of China (2014CB953802), the National Natural Science Foundation of China (40105012) and the Russian Scientific Fund under grant 14-47-00049. The authors thank the reviewer for valuable comments and suggestions.

References

- Allen L, Lindberg F, Grimmond CSB (2011) Global to city scale urban anthropogenic heat flux: model and variability. *Int J Climatol* 31(13):1990–2005
- Arnfield A (2003) Two decades of urban climate research: a review of turbulence, exchanges of energy and water, and the urban heat island. *Int J Climatol* 23:1–26
- Azorin-Molina C, Vicente-Serrano SM, TR MV, Jerez S, Sanchez-Lorenzo A, et al (2014) Homogenization and assessment of observed near-surface wind speed trends over Spain and Portugal, 1961–2011*. *J Clim* 27(10):3692–3712
- Block A, Keuler K, Schaller E (2004) Impacts of anthropogenic heat on regional climate patterns. *Geophys Res Lett* 31(12). doi:[10.1029/2004GL019852](https://doi.org/10.1029/2004GL019852)
- Bohnenstengel SI, Hamilton I, Davies M, Belcher SE (2014) Impact of anthropogenic heat emissions on London’s temperatures. *Quart J Roy Meteorol Soc* 140(679):687–698
- Bornstein R, Lin QL (2000) Urban heat islands and summertime convective thunderstorms in Atlanta: three cases studies. *Atmos Environ*. doi:[10.1016/S1352-2310\(99\)00374-X](https://doi.org/10.1016/S1352-2310(99)00374-X)
- Chen F, Mitchell K, Schaake J, Xue YK, et al (1996) Modeling of land-surface evaporation by four schemes and comparison with FIFE observations. *J Geophys Res* 101:7251–7268
- Chen F, Janjic Z, Mitchell K (1997) Impact of atmospheric surface layer parameterization in the new land-surface scheme of the NCEP mesoscale Eta numerical model. *Bound-Layer Meteorol* 85:391–421. doi:[10.1023/A:1000531001463](https://doi.org/10.1023/A:1000531001463)

- Chen F, Kusaka H, Bornstein R, et al (2011) The integrated WRF/urban modeling system: development, evaluation, and applications to urban environmental problems. *I Int J Climatol* 31(2):273–288
- Chen F, Yang XC, Zhu WP (2014) WRF simulations of urban heat island under hot-weather synoptic conditions: the case study of Hangzhou city, china. *Atmos Res* 138:364–377
- Dai YF, Liu YM, Zhou LJ (2011) Observation analysis of urbanization effect on surface air temperature trends in East China. *J Meteorol Sci* 31(4):365–371
- Della-Marta PM, Haylock MR, Luterbacher J, Wanner H (2007) Doubled length of western European summer heat waves since 1880. *J Geophys Res* 112:D15103. doi:[10.1029/2007JD008510](https://doi.org/10.1029/2007JD008510)
- Dudhia J (1989) Numerical study of convection observed during the winter monsoon experiment using a mesoscale two-dimensional model. *J Atmos Sci* 46:3077–3107
- Feng JM, Wang YL, Ma ZG, Liu YH (2012) Simulating the regional impacts of urbanization and anthropogenic heat release on climate across China. *J Clim* 25(20):7187–7203. doi:[10.1175/JCLI-D-11-00331.1](https://doi.org/10.1175/JCLI-D-11-00331.1)
- Feng JM, Wang J, Yan ZW (2014) Impact of anthropogenic heat release on regional climate in three vast urban agglomerations in China. *Adv Atmos Sci* 31(2):363–373
- Ferretti R, Mastrantonio G, Argentini S, Santoleri R, Viola A (2003) A model-aided investigation of winter thermally driven circulation on the Italian Tyrrhenian coast: a case study. *J Geophys Res-Atmospheres* 108:4777. doi:[10.1029/2003JD003424](https://doi.org/10.1029/2003JD003424)
- Fischer EM, Oleson WK, Lawrence DM (2012) Contrasting urban and rural heat stress responses to climate change. *Geophys Res Lett* 39:L03705. doi:[10.1029/2011GL050576](https://doi.org/10.1029/2011GL050576)
- Giannaros TM, Melas D, Daglis IA, Keramitsoglou I, Kourtidis K (2013) Numerical study of the urban heat island over Athens (Greece) with the WRF model. *Atmos Environ* 73:103–111
- Giovannini L, Zardi D, de Franceschi M, Chen F (2014) Numerical simulations of boundary-layer processes and urban-induced alterations in an Alpine valley. *Int J Climatol* 34(4):1111–1131
- Grawe D, Thompson HL, Salmond JA, Cai XM, Schlünzen KH (2013) Modeling the impact of urbanization on regional climate in the Greater London Area. *Int J Climatol* 33(10):2388–2401
- Grell GA, Devenyi D (2002) A generalized approach to parameterizing convection combining ensemble and data assimilation techniques. *Geophys Res Lett* 29:1693
- Guo H, Xu M, Hu Q (2011) Changes in near-surface wind speed in China: 1969–2005. *Int J Climatol* 31:349–358. doi:[10.1002/joc.2091](https://doi.org/10.1002/joc.2091)
- Hong SY, Yign N, Jimy D (2006a) A new vertical diffusion package with an explicit treatment of entrainment processes. *Mon Wea Rev* 134:2318–2341
- Hong SY, Lim JOJ (2006b) The WRF single-moment 6-class micro-physics scheme (WSM6). *J Korean Meteor Soc* 42:129–151
- Hu XM, Nielsen-Gammon JW, Zhang F (2010) Evaluation of three planetary boundary layer schemes in the WRF model. *J Appl Meteorol Clim* 49(9):1831–1844
- Jin ML, Shepherd JM (2005) Inclusion of urban landscape in a climate model: how can satellite data help? *Bull Am Meteorol Soc* 86:681–689. doi:[10.1175/BAMS-86-5-681](https://doi.org/10.1175/BAMS-86-5-681)
- Jones PD, Groisman PY, Coughlan M, Plummer N, Wang WC, Karl TR (1990) Assessment of urbanization effects in time series of surface air temperature over land. *Nature* 347(6289):169–172
- Jones PD, Lister DH, Li Q (2008) Urbanization effects in large-scale temperature records, with an emphasis on China. *J Geophys Res* 113:D16122. doi:[10.1029/2008JD009916](https://doi.org/10.1029/2008JD009916)
- Kang HQ, Zhu B, Zhu T, Sun JL, Ou JJ (2014) Impact of Megacity Shanghai on the urban heat-island effects over the downstream city kunshan. *Bound-Layer Meteor* 152:411–462. doi:[10.1007/s10546-014-9927-1](https://doi.org/10.1007/s10546-014-9927-1)
- Kalnay E, Cai M (2003) Impact of urbanization and land-use change on climate. *Nature* 423(6939):528–531
- Kjellstrom T, Kovats RS, Lloyd SJ, Holt T, Tol RS (2009) The direct impact of climate change on regional labor productivity. *Arch Environ Occup Health* 64(4):217–227. doi:[10.1080/19338240903352776](https://doi.org/10.1080/19338240903352776)
- Kusaka H, Kondo H, Kikegawa Y, Kimura F (2001) A simple single-layer urban canopy model for atmospheric models: comparison with multi-layer and slab models. *Bound-Layer Meteor* 101:329–358
- Kusaka H, Kimura F (2004) Coupling a single-layer urban canopy model with a simple atmospheric model: impact on urban heat island simulation for an idealized case. *J Meteor Soc Japan* 82:67–80
- Kusaka H, Nawata K, Suzuki-Parker A, Takane Y, Furuhashi N (2014) Mechanism of precipitation increase with urbanization in Tokyo as revealed by ensemble climate simulations. *J Appl Meteorol Clim* 53(4):824–839
- Lee SH, Song CK, Baik JJ, Park SU (2009) Estimation of anthropogenic heat emission in the Gyeong-Inregion of Korea. *Theor Appl Climatol* 96:291–303
- Li XX, Koh TY, Entekhabi D, Roth M, Panda J, Norford LK (2013) A multi-resolution ensemble study of a tropical urban environment and its interactions with the background regional atmosphere. *J Geophys Res Atmos* 118:9804–9818. doi:[10.1002/jgrd.50795](https://doi.org/10.1002/jgrd.50795)
- Lin CY, Chen F, Huang JC, Chen WC, Liou YA, Chen WN, Liu SC (2008) Urban heat island effect and its impact on boundary layer development and land-sea circulation over northern Taiwan. *Atmos Environ* 42:5635–5649
- Lin CY, Chen WC, Chang PL, Sheng FY (2011) Impact of the urban heat island effect on precipitation over a complex geographic environment in northern Taiwan. *J Appl Meteorol Climatol* 50:339–353. doi:[10.1175/2010JAMC2504.1](https://doi.org/10.1175/2010JAMC2504.1)
- Martine G, Marshall A (2007) State of world population 2007: Unleashing the potential of urban growth. Report. U. N. Popul Fund, New York
- McMichael AJ, Woodruff RE, Hales S (2006) Climate change and human health: present and future risks. *Lancet* 367:859–869. doi:[10.1016/S0140-6736\(06\)68079-3](https://doi.org/10.1016/S0140-6736(06)68079-3)
- Meehl GA, Tebaldi C (2004) More intense, more frequent, and longer lasting heat waves in the 21st century. *Science* 305:994–997
- Miao JF, Chen D, Borne K (2007) Evaluation and comparison of Noah and Pleim-Xiu land surface models in MM5 using GÖTE2001 data: spatial and temporal variations in near-surface air temperature. *J Appl Meteorol Clim* 46(10):1587–1605
- Miao SG, Chen F, LeMone MA, Tewari M, Li QC, Wang YC (2009) An observational and modeling study of characteristics of urban heat island and boundary layer structures in Beijing. *J Appl Meteorol Climatol* 48(3):484–501
- Miao SG, Chen F, Li QC, Fan SY (2011) Impacts of urban processes and urbanization on summer precipitation: a case study of heavy rainfall in Beijing on 1 August 2006. *J Appl Meteorol Climatol* 50:806–825. doi:[10.1175/2010JAMC2513.1](https://doi.org/10.1175/2010JAMC2513.1)
- Mlawer Eli J, Taubman Steven J, Brown Patrick D, et al (1997) Radiative transfer for inhomogeneous atmospheres: RRTM, a validated correlated-k model for the longwave. *J Geophys Res* 102:16663–16682
- Narumi D, Kondo A, Shimoda Y (2009) Effects of anthropogenic heat release upon the urban climate in a Japanese megacity. *Environ Res* 109(4):421–431
- Oleson KW, Bonan BG, Feddema J, Jackson T (2010) An examination of urban heat island characteristics in a global climate model. *Int J Climatol* 31:1848–1865. doi:[10.1002/joc.2201](https://doi.org/10.1002/joc.2201)
- Papanastasiou DK, Melas D, Lissaridis I (2010) Study of wind field under sea breeze conditions: an application of WRF model. *Atmos Res* 98(1):102–117
- Parker DE (2006) A demonstration that large-scale warming is not urban. *J Clim* 19(12):2882–2895. doi:[10.1175/JCLI3730.1](https://doi.org/10.1175/JCLI3730.1)

- Ren GY, Chu ZY, Chen ZH, Ren YY (2007) Implications of temporal change in urban heat island intensity observed at Beijing and Wuhan stations. *Geophys Res Lett.* doi:[10.1029/2006GL027927](https://doi.org/10.1029/2006GL027927)
- Salamanca F, Martilli A, Yagüe C (2012) A numerical study of the urban heat island over Madrid during the DESIREX (2008) campaign with WRF and an evaluation of simple mitigation strategies. *Int J Climatol* 32(15):2372–2386
- Shastri H, Paul S, Ghosh S, Karmakar S (2014) Impacts of urbanization on Indian summer monsoon rainfall extremes. *J Geophys Res Atmos.* doi:[10.1002/2014JD022061](https://doi.org/10.1002/2014JD022061)
- Sherwood S, Huber M (2010) An adaptability limit to climate change due to heat stress. *Proc Natl Acad Sci USA* 107(21):9552–9555. doi:[10.1073/pnas.0913352107](https://doi.org/10.1073/pnas.0913352107)
- Skamarock WC et al (2008) A description of the Advanced Research WRF version 3. NCAR Tech Note NCAR/TN-475STR 125 pp. http://www.mmm.ucar.edu/wrf/users/docs/arw_v3.pdf
- Tran H, Uchihama D, Ochi S, Yasuoka Y (2006) Assessment with satellite data of the urban heat island effects in Asian mega cities. *Int J Appl Earth Observ Geoinform* 8(1):34–48
- Wan HC, Zhong Z, Yang XQ, Li XQ (2012) Ensembles to model the impact of urbanization for a summertime rainstorm process in Yangtze river delta, china. *Meteorol Appl* 22:105–112. doi:[10.1002/met.1360](https://doi.org/10.1002/met.1360)
- Wang GC, Li LQ, Wang Y, Xuan YJ, Wan XW, Kong QX, Chen HB (2004) XLS-II tethered balloon sounding system. *Meteorol Sci Technol* 32(4):269–273
- Wang HZ, Sun JN, Zhu LF, Liu P, Shen LD (2013a) Correction of wind speed measured by tethered balloon sounding system and application to evaluation the data from wind profile radar. *J Meteorol Sci* 33(5):485–491. doi:[10.3969/2012jms.0180](https://doi.org/10.3969/2012jms.0180)
- Wang J, Feng JM, Yan ZW, Hu YH, Jia GS (2012) Nested high-resolution modeling of the impact of urbanization on regional climate in three vast urban agglomerations in China. *J Geophys Res* 117: D21103. doi:[10.1029/2012JD018226](https://doi.org/10.1029/2012JD018226)
- Wang MN, Yan XD, Liu JY, Zhang XZ (2013b) The contribution of urbanization to recent extreme heat events and a potential mitigation strategy in the Beijing–Tianjin–Hebei metropolitan area. *Theor Appl Climatol* 114:407–416
- Wang MN, Zhang XZ, Yan XD (2013c) Modeling the climatic effects of urbanization in the Beijing–Tianjin–Hebei metropolitan area. *Theor Appl Climatol* 113:377–385
- Wang SW, Cai JN, Mu QZ, et al (2002) Modeling and diagnostic studies on the variations of the subtropical high over the western Pacific from 1880 to 1999. *Adv Atmos Sci* 19(6):1148–1152
- Wang XM, Liao JB, Zhang J, Shen C, Chen WH, Xia BC, Wang TJ (2014) A numeric study of regional climate change induced by urban expansion in the Pearl River Delta, China. *J Appl Meteorol Climatol* 53(2):346–362
- Willett KM, Sherwood S (2012) Exceedance of heat index thresholds for 15 regions under a warming climate using the wet-bulb globe temperature. *Int J Climatol* 32:161–177. doi:[10.1002/joc.2257](https://doi.org/10.1002/joc.2257)
- Xu YY, Liu SH, Hu F (2009) Influence of Beijing urbanization on the characteristics of atmospheric boundary layer. *Chinese J Atmos Sci* 33(4):859–867
- Yang L, Smith JA, Baeck ML, Bou-Zeid E, Jessup SM, Tian F, Hu H (2014) Impact of urbanization on heavy convective precipitation under strong large-scale forcing: a case study over the Milwaukee–Lake Michigan region. *J Hydrometeorol* 15(1):261–278
- Yu M, Liu YM, Dai YF, Yang AQ (2013) Impact of urbanization on boundary layer structure in Beijing. *Clim Chang* 120:123–136. doi:[10.1007/s10584-013-0788-2](https://doi.org/10.1007/s10584-013-0788-2)
- Zhang DL, Zheng WZ (2004) Diurnal cycles of surface winds and temperatures as simulated by five boundary layer parameterizations. *J Appl Meteorol* 43(1):157–169
- Zhang DL, Shou YX, Dickerson RR, Chen F (2011) Impact of upstream urbanization on the urban heat island effects along the Washington–Baltimore Corridor. *J Appl Meteorol Clim* 50(10):2012–2029
- Zhang N, Gao ZQ, Wang XM, Chen Y (2010a) Modeling the impact of urbanization on the local and regional climate in Yangtze River Delta, China. *Theor Appl Climatol* 102(3–4):331–342
- Zhang Y, Wen XY, Jang CJ (2010b) Simulating chemistry–aerosol–cloud–radiation–climate feedbacks over the continental US using the online-coupled Weather Research Forecasting Model with chemistry (WRF/Chem). *Atmos Environ* 44(29):3568–3582
- Zhang YZ, Miao SG, Dai YJ, Liu YH (2013) Numerical simulation of characteristics of summer clear day boundary layer in Beijing and impact of urban underlying surface on sea breeze. *Chinese J Geophys* 56(8):2558–2573. doi:[10.6038/cjg20130806](https://doi.org/10.6038/cjg20130806)